HHS Public Access

Author manuscript

Mol Cell Endocrinol. Author manuscript; available in PMC 2023 March 04.

Published in final edited form as:

Mol Cell Endocrinol. 2023 January 01; 559: 111781. doi:10.1016/j.mce.2022.111781.

Mediator subunit MED1 differentially modulates mutant thyroid hormone receptor intracellular dynamics in Resistance to Thyroid Hormone syndrome

Moyao Wang,

Vincent R. Roggero,

Lizabeth A. Allison*

Department of Biology, William & Mary, 540 Landrum Drive, Integrated Science Center 3030, Williamsburg, VA 23185, U.S.A.

Abstract

Thyroid hormone receptor (TR) controls the expression of thyroid hormone (T3)-responsive genes, while undergoing rapid nucleocytoplasmic shuttling. In Resistance to Thyroid Hormone syndrome (RTH), mutant TR fails to activate T3-dependent transcription. Previously, we showed that Mediator subunit 1 (MED1) plays a role in TR nuclear retention. Here, we investigated MED1's effect on RTH mutants using nucleocytoplasmic scoring and fluorescence recovery after photobleaching in transfected cells. MED1 overexpression and knockout did not change the nucleocytoplasmic distribution or intranuclear mobility of C392X and P398R TRα1 at physiological T3 levels. At elevated T3 levels, however, overexpression increased P398R's nuclear retention and MED1 knockout decreased P398R's and A263V's intranuclear mobility, while not impacting C392X. Although A263V TRα1-transfected cells had a high percentage of aggregates, MED1 rescued A263V's impaired intranuclear mobility, suggesting that MED1 ameliorates nonfunctional aggregates. Results correlate with clinical severity, suggesting that altered interaction between MED1 and TRα1 mutants contributes to RTH pathology.

Keywords

fluorescence recovery after photobleaching (FRAP); Mediator subunit 1 (MED1); nuclear receptor; nuclear localization; Resistance to Thyroid Hormone syndrome (RTH); thyroid hormone receptor

1. Introduction

Thyroid hormone receptor (TR) is a member of the nuclear receptor superfamily and mediates the effect of thyroid hormone (T3) by activating and repressing the transcription of hundreds of target genes. Hence, TR plays a vital role in human health by regulating many aspects of development, growth, and metabolism (Bassett & Williams, 2003; Brent,

*Corresponding author. laalli@wm.edu (L.A. Allison).

Conflicts of interest

The authors declare that there is no conflict of interest that could be perceived as prejudicing the impartiality of the research reported.

2012; Chávez et al., 1998; Contreras-Jurado et al., 2014; Dinda et al., 2002; Mullur et al., 2014; Pascual & Aranda, 2013; Preau et al., 2015; Puzianowska-Kuznicka et al., 2006: Qi et al., 1999; Stepien & Huttner, 2019; Williams, 2009; Wojcicka et al., 2013). The two major subtypes of TR, TRα1 and TRβ1, can bind to specific sequences on the DNA called thyroid hormone response elements (TREs) as monomers, homodimers, and heterodimers with the retinoid X receptor (RXR) (Laudet & Gronemeyer, 2002; Sap et al., 1986; Umesono & Evans, 1989; Weinberger et al., 1986). In the absence of T3, TR interacts with corepressors and represses transcription on positive TREs (Hollenberg et al., 1996; Hörlein et al., 1995; Koenig, 1998; Yoh & Privalsky, 2001). After binding T3, TR undergoes a conformational change that releases corepressors and recruits coactivators such as Mediator subunit 1 (MED1) to activate transcription (Femia et al., 2020; Figueira et al., 2011; Moras & Gronemeyer, 1998; Yuan et al., 1998).

Although TR functions as a transcription factor and mainly exerts its effects inside the nucleus, it shuttles rapidly between the nucleus and the cytoplasm (Bunn et al., 2001). The nuclear import and export of TR are mediated by interactions with importins and exportins, respectively (Zhang et al., 2018). Both TRα1 and TRβ1 have a classical nuclear localization signal 1 (NLS-1) in the hinge domain and at least three nuclear export signals (NESs) in the ligand binding domain (LBD), while TRα1 has an additional nonclassical NLS-2 in the A/B domain (Fig. 1) (Mavinakere et al., 2012; Salomon et al., 2020). One of the NESs, NES-H12, located in helix 12 of the LBD, overlaps with the activation function 2 (AF-2) domain and coactivator binding site (Mavinakere et al., 2012).

Mutations in TR lead to an inherited disease called Resistance to Thyroid Hormone syndrome (RTH), impacting about 1 in 40,000 people (Moran et al., 2014). Although mutations in the *THRB* gene cause almost all known cases of RTH syndrome, the first case of a *THRA* mutation was discovered in 2012 (Bochukova et al., 2012). RTH syndromes caused by TRα and TRβ gene mutations were later renamed as RTHα and RTHβ, respectively. To date, 27 RTH mutations have been identified in TRα1 (Bochukova et al., 2015; Chen et al., 2019; Demir et al., 2016; Espiard et al., 2015; Furman et al., 2017; Kalikiri et al., 2017; Korkmaz et al., 2019; le Maire et al., 2020; Moran et al., 2013, 2014, 2017; Paisdzior et al., 2021; Sun et al., 2019; Tylki-Szymańska et al., 2015; van Gucht et al., 2016, 2017; van Mullem et al., 2012; Yuen et al., 2015). RTHβ is usually diagnosed in patients by the presence of a goiter, while RTHα has a broader range of symptoms (Singh & Yen, 2017; Sun et al., 2020; Weiss & Refetoff, 2000). Due to the lack of distinct phenotype and largely normal thyroid function tests, RTHα often is undiagnosed (Moran et al., 2017). In both RTHα and RTHβ, the thyroid gland produces enough T3, but the mutant TRs are defective in T3 binding, blocking the conformational change required to recruit coactivators like MED1 (Ortiga-Carvalho et al., 2014).

MED1, also known as TRAP220, bridges TR to the Mediator complex, a large multi-protein complex required for transcription by RNA polymerase II (Pol II) (Liu et al., 2015; Soutourina et al., 2018). MED1 binds to the AF-2 domain of TR through the highly conserved LXXLL motif located in the two nuclear receptor boxes (NR boxes) or receptor binding domains (NBD) (Jin et al., 2012). MED1 has been shown to impact both intracellular dynamics of TR and TR-mediated gene transcription activity. MED1 knockout

mouse embryonic fibroblast (MEF) cells show impaired TR function, but the expression of MED1 in the MED1$^{-/-}$ MEFs restores TR function (Ito et al., 2000). Our previous research showed that there is a decrease in nuclear retention of TR in MED1$^{-/-}$ MEFs, and MED1 overexpression in HeLa (human) cells increases nuclear retention and decreases intranuclear mobility of TRβ1 (Femia et al., 2020). However, the interaction between MED1 and RTH mutants of TR was not investigated in our prior study.

Due to the importance of TR's helix 12 in the interaction with MED1, we hypothesized that two RTH helix 12 mutants, C392X and P398R, would be less responsive to MED1 levels compared to wild-type TRα1. P398R is a point mutation found in the middle of helix 12, while C392X is a missense mutation resulting in a premature stop codon, deleting most of helix 12 (Fig. 1). A263V, a point mutation in helix 6, away from the critical helix 12, was chosen to act as a control for mutant TR and MED1 interaction since the MED1 binding site on A263V TRα1 is unchanged. Previous research has shown that A263V and P398R mutants show reduced sensitivity to T3, while C392X loses almost all its ability to interact with T3 (Moran et al., 2014; Moran et al., 2017; Tylki-Szymańska et al., 2015; van Gucht et al., 2017). Hence, we hypothesized that T3 levels would also impact the interaction between mutant TR and MED1.

2. Materials and methods

2.1. Plasmids

Coding regions for human wild-type TRα1, A263V TRα1, A263S TRα1, C392X TRα1, and P398R TRα1 were acquired from Invitrogen GeneArt Gene Synthesis (Thermo Fisher Scientific) and subcloned into pmCherry-C1 (Clontech). GFP-MED1 was obtained from Origene Technologies, Inc and encodes full-length human MED1 (residues 1-1581). GFP-NCoR1 and GFP-MED13 were acquired from GenScript and GeneCopoeia, respectively. The GFP-250 expression vector encodes the well-established aggresome marker GFP-250, composed of GFP fused at its C-terminus to the first 250 amino acids of p115, a protein involved in the transport of cargo from the endoplasmic reticulum to the Golgi (Salomon et al., 2020).

2.2. Cell culture and transient transfection

HeLa cells (#CCL-2; American Type Culture Collection) were grown in minimum essential medium (MEM; Gibco) supplemented with 10% fetal bovine serum (FBS; Gibco) at 37°C under 5% CO_2 and 98% humidity. MED1$^{+/+}$ and MED1$^{-/-}$ mouse embryonic fibroblasts (MEFs) were a gift from Dr. Robert Roeder, Rockefeller University (Ito et al., 2000). MEFs were grown in Dulbecco's Modified Eagle Medium (DMEM; Gibco) supplemented with 10% newborn calf serum (NBCS; Gibco) at 37°C under 5% CO_2 and 98% humidity. Cells were seeded at a density of 2.5×10^5 cells per well and transfected using Lipofectamine 3000 (Invitrogen) 24 h later. Six hours post-transfection, the transfection mixtures were replaced by MEM supplemented with 10% FBS or DMEM supplemented with 10% NBCS. For thyroid hormone (T3) treatment, the transfection mixtures were replaced by MEM or DMEM supplemented with 10% charcoal-stripped FBS (Gibco) and with or without 100 nM T3 (MilliporeSigma).

2.3. Nucleocytoplasmic distribution and aggregate analysis

Cells were fixed in 3.7% formaldehyde 24 h post-transfection. Coverslips (22mm, round; Thermo Fisher Scientific) were mounted on glass slides using Fluoro-Gel II containing DAPI (Electron Microscopy Sciences). Fluorescence images were taken using All-in-One Fluorescence Microscope BZ-X800 (Keyence America). Protein distribution was analyzed using Icy. Regions of interest (ROIs) were selected both inside the nucleus and cytoplasm of cells. The nuclear-cytoplasmic (N/C) ratio was calculated by dividing the fluorescence intensity inside the nucleus by the fluorescence intensity inside the cytoplasm. The normalized N/C ratio was calculated by normalizing the treatment group to corresponding wild-type controls. A relatively higher raw N/C ratio indicates a more nuclear distribution, while a relatively lower raw N/C ratio indicates a more cytoplasmic distribution.

In addition, the presence of nuclear and cytoplasmic aggregates was assessed qualitatively to determine the percentage of cells with or without aggregation for A263V and A263S mutants. Two main phenotypes were defined: 1) “No aggregation” refers to a homogeneous distribution of TR within a cell, without bright fluorescent foci, and 2) “Aggregation” refers to cells with bright fluorescent foci of TR, ranging from speckles to larger aggregates. Each experiment contained at least three biologically independent replicates with 60 cells scored per replicate. For analysis of colocalization of the aggresome marker GFP-250 with mCherry-tagged wild-type TR and the A263V mutant, cotransfected HeLa cells were imaged by confocal microscopy.

2.4. Fluorescence recovery after photobleaching (FRAP)

Cells were washed with Dulbecco’s phosphate-buffered saline (D-PBS) and incubated in MEM-α with or without 100 nM T3 (MilliporeSigma) in an OkoLab Incubation System (Warner Instruments, Inc) at 37°C and 5% CO_2. Strip-fluorescence recovery after photobleaching (Strip-FRAP) was performed using a Nikon A1Rsi confocal microscope Ti-E-PFS (Nikon, Inc) with a ×60 oil objective and perfect focus system. The 488-nm line and 561-nm line of krypton-argon lasers were used for GFP and mCherry detection, respectively. A solid-state 405-nm laser was used for photobleaching. Acquisition and photobleaching were achieved in Nikon NIS-Elements AR Software (Nikon). Using the ROI module, one stimulation line region of interest (ROI) positioned horizontally across the nucleus and two acquisition ROIs placed inside the nucleus and outside of the cell, respectively, were created. The total experimental time for the assay was set to 35 s using the A1 plus stimulation module of NIS-Elements. With a frame rate at approximately 15.3 frames/s, 535 frames were collected in total. The total experimental time was divided into a 5-s pre-bleach acquisition phase at approximately 2 to 3% laser power, a 1-s photobleaching phase at 100% laser power on a stimulation line ROI, and a 29-s post-bleach acquisition phase at approximately 2 to 3% laser power. All image acquisition was conducted through resonant scanning, corrected by line averaging. Fluorescence intensities for the stimulation line ROI and two acquisition ROIs were recorded for each frame. Each experiment contained three biologically independent replicates with 20 nuclei analyzed per replicate.

Although strip-FRAP does not allow calculation of a diffusion constant, it is better at reducing experimental noise due to diffusion during the bleaching process for a fast-moving

protein like TRα1 (González-Pérez et al., 2011). Since TRα1 does not localize to the nucleolus, we avoided drawing the bleach strip across the nucleolus, although it has been shown that placing the bleach strip this way does not affect the recovery rate of another transcription factor, Smad2 (González-Pérez et al., 2011). To better analyze the FRAP recovery curve, we employed a double-term exponential fit strategy outlined in Firmino et al. (2013). We also compared the double exponential fit model to single exponential fit model using Akaike information criterion (AIC) and Bayesian information criterion (BIC), where we saw a more than 99.99% chance that the double exponential fit model is the better one as determined by AIC. We also compared the double exponential fit model to the triple exponential fit model using AIC and BIC, where again, we saw a more than 99.99% chance that the double exponential fit is the better model.

FRAP data were first double normalized as described by Phair et al. (2004) to correct for background fluorescence intensity and the loss of fluorescence intensity due to photobleaching. The double normalized data were then fully normalized using the strategy described in Femia et al. (2020). The fully normalized data ranged from 0 to 1, where 0 represents the lowest fluorescence intensity directly after the photobleaching phase, and 1 represents the average fluorescence intensity of the pre-bleach acquisition phase and the maximum recovery possible in the post-bleach acquisition phase. The fully normalized data were then fitted using a two-term exponential fit (equation 1), where τ_1 and τ_2 ($\tau_1 < \tau_2$) represent the time constant for the faster and slower recovery process, respectively. C_1 and C_2 represent the fraction of proteins that contributed to the faster and slower recovery, respectively.

$$f_{(t)} = C_1\left(1 - e^{-\frac{t}{\tau_1}}\right) + C_2\left(1 - e^{-\frac{t}{\tau_2}}\right) \quad (1)$$

The fitted C_1, C_2, τ_1, and τ_2 were used to calculate mobile (equation 2) and immobile fractions (equation 3). The mobile fraction represents the fraction of proteins capable of moving inside the nucleus, whereas the immobile fraction represents the population of proteins that are not able to move as a result of DNA binding, formation of aggregates, or interaction with other nuclear factors. The mobile and immobile fractions are two of the primary parameters used to evaluate changes in intranuclear mobility.

$$F_{mobile} = C_1 + C_2 \quad (2)$$

$$F_{immobile} = 1 - F_{mobile} \quad (3)$$

The third primary parameter used to evaluate changes in intranuclear mobility is $t_{1/2}$, which represents the time taken to reach 50% of the maximum recovery for each replicate. $t_{1/2}$ was acquired by solving equation 4 with fitted C_1, C_2, τ_1, and τ_2.

$$\frac{C_1 + C_2}{2} = C_1\left(1 - e^{-\frac{t_{1/2}}{\tau_1}}\right) + C_2\left(1 - e^{-\frac{t_{1/2}}{\tau_2}}\right) \quad (4)$$

2.5. Luciferase reporter gene assay

HeLa cells were seeded at 2.0×10^4 cells per well in a white 96-well plate (PerkinElmer). Twenty- four hours after seeding, cells were transiently transfected with expression plasmids for GFP-TRα1 wild-type or RTH mutants, TRE (DR+4)-firefly luciferase reporter, and Renilla luciferase internal control. Five hours post-transfection, medium was replaced with MEM containing 10% charcoal-stripped FBS, supplemented or not with 100 nM T3. After an additional 19 h, a Dual-Glo® Luciferase Assay (Promega) was performed, according to the manufacturer's protocol. Three independent, biologically separate replicate experiments were performed, with 8 wells assayed per treatment.

2.6. Statistical analysis

All data are expressed as mean ± SEM. All p values were calculated using two-tailed t-tests, and p values less than 0.05 were considered statistically significant.

3. Results

3.1. Knockout of MED1 does not alter the nuclear localization patterns of TRα1 mutants under physiological T3 levels

Although primarily localized to the nucleus at steady state, TRα1 shuttles rapidly between the nucleus and the cytoplasm (Bunn et al., 2001). Nuclear import and nuclear export are facilitated by importins and exportins, respectively (Zhang et al., 2018). Our previous research has shown that knockout of MED1 decreases the nuclear retention of wild-type TRα1 (Femia et al., 2020). To investigate the impact of MED1 on mutant TRα1, we used our well characterized and validated transient transfection assays in wild-type ($MED1^{+/+}$) and knockout ($MED1^{-/-}$) mouse embryonic fibroblasts (MEFs). We have previously shown that fluorescent protein tags do not alter the localization patterns of TRα1, and that overexpression of TRα1 does not overload the nuclear import and export pathways (Femia et al., 2020). Since all mutant TRs we selected show reduced T3 sensitivity (Moran et al., 2014; Moran et al., 2017; Tylki-Szymańska et al., 2015; van Gucht et al., 2017), we hypothesized that MED1 knockout would not alter the intracellular localization patterns of TRα1 RTH mutants under the T3 levels that naturally exist in culture medium supplemented with newborn calf serum, referred to hereinafter as “physiological” T3 levels. To test our hypothesis, mCherry-tagged A263V, C392X, and P398R TRα1 were transfected into $MED1^{+/+}$ and $MED1^{-/-}$ MEFs, and the average relative nuclear to cytoplasmic (N/C) ratio was quantified using fluorescence intensities determined by fluorescence microscopy.

Similar to our previous study (Femia et al., 2020), wild-type TRα1 was highly nuclear localized in $MED1^{+/+}$ cells, with only less than 10% of the total protein population localized to the cytoplasm, whereas knockout of MED1 in $MED1^{-/-}$ MEFs significantly decreased the nuclear population of wild-type TRα1 (Fig. 2A and 2E). The average relative N/C ratio of TRα1 in $MED1^{-/-}$ MEFs was approximately 13% less than $MED1^{+/+}$ MEFs,

indicating a significantly greater cytoplasmic localization ($p<0.001$). As predicted, $MED1^{-/-}$ knockout did not significantly alter the N/C ratios of the RTHα mutants, P398R TRα1 (Fig. 2B and 2E), C392X TRα1 (Fig. 2C and 2E), or A263V TRα1 (Fig. 2D and 2E), when compared to their N/C ratios in the $MED1^{+/+}$ MEFs ($p>0.05$). In addition, the N/C ratios of all three RTHα mutants were not statistically significantly different from wild-type TRα1 as determined by two tailed t-tests ($p>0.05$). These data suggest that MED1 does not functionally interact with TRα1 mutants under physiological T3 levels. Although it could be postulated that the N/C ratios of the RTHα mutants in $MED1^{+/+}$ MEFs should be the same as wild-type TRα1 in the $MED1^{-/-}$ MEFs, RTHα mutant receptors also may bind nuclear corepressor 1 (NCoR1) with higher affinity and dissociate more slowly than the wild-type receptor in the presence of T3 (Fozzatti et al., 2013). Such an altered interaction with NCoR1 could promote enhanced nuclear retention of the RTHα mutants, countering the effects of a lack of interaction with MED1.

3.2. Overexpression of MED1 increases the nuclear population of P398R TRα1 when supplemented with 100 nM T3

Our previous research has shown that overexpression of MED1 increases the nuclear retention of wild-type TRβ1 in human (HeLa) cells; however, any comparable increase in nuclear retention of wild-type TRα1 was not measurable, since wild-type TRα1 is already highly nuclear-localized (Femia et al., 2020). To test the effect of MED1 overexpression on RTHα mutants, we employed our well-established transient transfection assays in HeLa cells. HeLa cells provide a robust model system for several reasons. They do not express detectable levels of endogenous TR, so the impact of endogenous receptors on distribution patterns through heterodimerization does not have to be taken into account, but the cells are still responsive to T3 when TR is introduced. In addition, exogenous wild-type TR is primarily nuclear-localized over a wide range of expression levels, overexpression does not lead to non-specific protein aggregation or saturation of the nuclear transport machinery, and fluorescent tags do not alter localization patterns (Femia et al., 2020; Salomon et al., 2020).

Since the three RTHα mutants we selected show reduced T3 sensitivity (Lindl, 2002; Moran et al., 2014; Moran et al., 2017; Tylki-Szymańska et al., 2015; van Gucht et al., 2017), we hypothesized that MED1 overexpression would not impact their intracellular localization patterns under ~1.2 nM T3, which is the level of T3 naturally supplemented by fetal bovine serum (FBS) in the culture medium, hereinafter referred to as “physiological” T3 levels. Since research has reported that 100 nM T3 is enough to elicit a transcriptional response in certain RTHα mutants (Moran et al., 2014; Moran et al., 2017), we further hypothesized that MED1 overexpression would alter the intracellular localization patterns of RTHα mutants in the presence of 100 nM T3, added to charcoal-stripped FBS. We also predicted that MED1 overexpression would increase the nuclear population of P398R but not C392X TRα1 since P398R is a less severe point mutation, whereas C392X has lost almost the entire MED1 binding site (see Fig. 1). To test our hypotheses, mCherry-tagged wild-type TRα1, and A263V, C392X, and P398R TRα1 RTH mutants were either single-transfected or cotransfected with GFP-tagged MED1 into HeLa cells in the absence of T3, or in the presence of physiological T3 (1.2 nM) or elevated T3 (100 nM) levels, and the average relative N/C ratios for wild-type and mutant TRα1 were calculated.

As in our previous study (Femia et al., 2020), MED1 overexpression did not impact the intracellular localization of wild-type TRα1 (Fig. 3A and 3B). Moreover, cells transfected with GFP-MED1 alone showed fluorescent foci similar to those previously reported by us and other labs (Femia et al., 2020; Sabari et al., 2018; Shi et al., 2021) and, notably, these MED1 foci disappeared when coexpressed with TRα1, forming a homogeneous distribution of both proteins. As predicted, MED1 overexpression did not change the intracellular localization patterns of P398R TRα1 (Fig. 3C and 3D) and C392X TRα1 (Fig. 3E and 3F) under physiological (~1.2 nM) T3 levels ($p>0.05$). In addition, C392X and P398R TRα1 showed no differences in the average relative N/C ratio compared to wild-type TRα1 when transfected alone ($p>0.05$).

In contrast, in the presence of 100 nM T3, MED1 overexpression significantly altered the intracellular localization pattern of P398R TRα1 (Fig. 3C and 3D). On average, the relative N/C ratio for P398R TRα1 cotransfected with MED1 showed an approximately 14% increase compared to single-transfected P398R TRα1 ($p<0.01$). Not surprisingly, MED1 overexpression did not alter the intracellular localization pattern of C392X TRα1, which lacks all of helix 12 ($p>0.05$) (Fig. 3E and 3F). Taken together, these data further support our model that the interaction between MED1 and RTH mutant TRα1 is impaired under physiological T3 levels. The interaction between MED1 and TRα1 with the less severe P398R mutation can be restored when supplemented with T3, while the interaction between MED1 and TRα1 with the more catastrophic C392X mutation is still impaired even after providing elevated T3 levels.

3.3. Overexpression of MED1 increases the percentage of A263V TRα1 transfected cells with aggregates

Due to the presence of aggregates of A263V TRα1 in transfected HeLa cells, we were unable to accurately quantify N/C ratios in MED1-cotransfected cells, as was done for the P398R and C392X mutants (see Fig. 3). A263V TRα1 formed both nuclear and cytoplasmic foci, ranging in size from small speckles to larger aggregates, suggesting misfolding of A263V TRα1 (Fig. 4A, rows 1-4). To quantify aggregate formation, we calculated the average percentage of cells with either nuclear or cytoplasmic aggregates in A263V and wild-type TRα1 under various transfection schemes and T3 levels. Expressing A263V instead of wild-type TRα1 in HeLa cells significantly increased the percentage of cells with aggregates, and more interestingly, overexpressing MED1 with A263V TRα1 shifted the percentage even higher (Fig. 4B). On average, A263V TRα1 transfected cells showed a five-fold increase in the percent of cells with aggregates compared to wild-type TRα1 ($p<0.05$), and A263V TRα1 and MED1 cotransfected cells almost doubled the percentage of cells with aggregates compared to A263V TRα1 single-transfected cells ($p<0.01$). Not surprisingly, $MED1^{-/-}$ knockout significantly decreased the percentage of cells with aggregates of A263V TRα1, while the same effect was not seen in wild-type TRα1 (Fig. 4D). The average percent of cells with aggregates was approximately 50% higher in A263V transfected $MED1^{+/+}$ MEFs than $MED1^{-/-}$ MEFs ($p<0.05$).

We then tested how changes in T3 levels impact aggregate formation. We hypothesized that by providing 100 nM T3, A263V TRα1 would be able to bind to T3, which would lead

to a conformational change in A263V TRα1 and weaken the protein-protein interaction within the aggregates, disfavoring aggregate formation. As predicted, supplementing with 100 nM T3 decreased the percentage of HeLa cells with aggregates for both A263V TRα1 single-transfection and A263V TRα1 and MED1 cotransfection, supporting our hypothesis (Fig. 4C). On average, T3-supplemented A263V TRα1 transfected cells showed a 57% decrease in aggregate formation compared to T3-depleted cells, while T3 supplemented A263V TRα1 and MED1 cotransfected cells showed a 34% decrease in aggregate formation compared to T3 depleted cells ($p<0.05$). Again, we did not see any significant amount of aggregation in both T3 supplemented and T3 depleted WT TRα1 transfected cells ($p>0.05$).

We had previously shown that MED13, although to a lesser extent than MED1, also impacts the nuclear retention of WT TRα1 (Femia et al., 2020). To test whether other proteins in the Mediator complex also induce A263V TRα1 aggregate formation, we cotransfected A263V TRα1 with GFP-MED13 into HeLa cells. Approximately 20% of cells cotransfected with A263V TRα1 and MED13 contained nuclear or cytoplasmic aggregates (Fig. 4A, row 5). This finding led us to hypothesize that A263V TRα1 interacts with Mediator complex subunits non-specifically, possibly through the intrinsically disordered domains that are proposed to contribute to the organization of the Mediator complex (Boija et al., 2018; Palacio & Taatjes, 2022). To further test our hypothesis, we cotransfected HeLa cells with A263V TRα1 and NCoR1, a corepressor that interacts with wild-type TRα1 but is not a component of the Mediator complex (Hörlein et al., 1995). Supporting our hypothesis, A263V TRα1 and NCoR1 cotransfected cells showed a homogeneous distribution of both proteins without any aggregates (Fig. 4A, panel 7). Taken together, these results suggest that MED1 and MED13 could interact with A263V TRα1 in a non-specific fashion and potentially form aggregates with A263V TRα1 through the intrinsically disordered domains contained in many subunits of the Mediator complex (Nagulapalli et al., 2016).

In our previous studies, we observed that 23% of HeLa cells transfected with K74E, A264V TRα1, a mutant isolated from hepatocellular carcinoma (HCC) patients, also formed nuclear and cytoplasmic aggregates (Salomon et al., 2020). We then questioned whether mutations around the A263 position in the NES-H6 region are highly favorable to aggregate formation. To test this hypothesis, we cotransfected Hela cells with MED1 and another RTH mutant, A263S TRα1. As predicted, about 15% of A263S TRα1 and MED1 cotransfected cells showed both nuclear and cytoplasmic aggregates (Figure 4D, panel 6). Further supporting our hypothesis, another cancer-associated mutant, L251P, which resides in the NES-H6 region, also showed increased aggregate formation (Salomon et al., 2020). Given our prior results showing that cancer-associated mutants of TR often form aggregates that can subsequently be recruited by a microtubule-dependent mechanism to the perinuclear aggresome (Salomon et al., 2020), we sought to further explore the nature of the aggregates formed by A263V. To this end, we examined colocalization with GFP-250, a well-established aggresome marker. Wild-type TRα1 was primarily nuclear and did not colocalize with GFP-250, which was localized in the cytoplasm (Fig. 4E, upper panels). In contrast, cytoplasmic aggregates of A263V showed colocalization with GFP-250, suggesting that some of these aggregates are being recruited to the aggresome (Fig. 4E, lower panels). Overall, these data suggest that TRα1 with mutations in the NES-H6 region of helix 6 is more prone to aggregation.

3.4. MED1 overexpression partially rescues the impaired nuclear mobility of A263V TRα1

We previously investigated the effect of MED1 overexpression on the intranuclear mobility of wild-type TRα1 using an alternative FRAP technique called strip-FRAP that involves photobleaching a strip drawn across the entire length of the nucleus and recording the fluorescence recovery in the strip over time (Femia et al., 2020). Here, we used strip-FRAP to further investigate the properties of A263V TRα1 aggregates under physiological T3 levels.

As shown in Fig. 5A (rows 2 and 3), aggregates (bright foci) were present in the A263V transfected cells analyzed by strip-FRAP. As predicted, A263V TRα1 showed a significantly slower intranuclear mobility profile than wild-type TRα1 (Fig. 5A and 5B). The average $t_{1/2}$ was 1.045 s for wild-type TRα1 compared to 1.403 s for A263V TRα1 (Table 1; $p<0.001$). In addition, A263V TRα1 also showed a significant decrease of 29% in the mobile fraction compared to wild-type TRα1 (Table 1; $p<0.001$). This reduction in the mobile fraction is contributed by the short-term or immediate recovery process represented by C_1 (see Materials and Methods, equations 1-4) ($p<0.001$). In contrast, the fraction of the long-term or gradual recovery process described by C_2 for A263V TRα1 is surprisingly higher than for wild-type TRα1 (Table 1; $p<0.05$). However, the time constants for wild-type TRα1 and A263V TRα1 are not significantly different for either the short-term or long-term recovery processes represented by $\tau 1$ and $\tau 2$, respectively (Table 1; $p>0.05$).

Notably, even though MED1 coexpression increased the percent of A263V-transfected cells with aggregates, MED1 coexpression also increased the intranuclear mobility of A263V TRα1. A263V TRα1 aggregates showed a much slower recovery time than MED1 and A263V TRα1 co-aggregates (Fig. 5A, rows 2 and 3). The average $t_{1/2}$ was 1.403 s for A263V TRα1 compared to 1.126 s for A263V TRα1 coexpressed with MED1 (Table 1; $p<0.001$). More importantly, the $t_{1/2}$ for A263V TRα1 coexpressed with MED1 is not significantly different from wild-type TRα1 (Table 1; $p>0.05$). MED1 coexpression also increased the mobile fraction of A263V TRα1 by approximately 25% ($p<0.001$), but not to the level of wild-type TRα1 ($p<0.05$); however, the effect was mainly caused by an increase in the fraction responsible for short-term recovery as MED1 coexpression significantly increased the C_1 parameter in the FRAP profile ($p<0.01$). The fraction responsible for the long-term recovery represented by C_2 was not significantly different between A263V TRα1 and A263V TRα1 coexpressed with MED1 ($p>0.05$), and the C_2 of A263V TRα1 coexpressed with MED1 was still significantly greater than wild-type TRα1 ($p<0.01$). Again, there were no significant differences in both time constants (τ_1 and τ_2) between A263V TRα1 and A263V TRα1 coexpressed with MED1, or A263V TRα1 coexpressed with MED1 and wild-type TRα1 ($p>0.05$). Taken together, these results show that MED1 can interact with A263V TRα1 even at physiological T3 levels, and overexpression of MED1 partly rescues the impaired intranuclear mobility of A263V TRα1 in terms of $t_{1/2}$, suggesting that MED1 can form relatively more dynamic and potentially functional complexes with A263V TRα1.

To further investigate the interactions between MED1 and RTHα mutants, we also tested the intranuclear mobility profile for C392X and P398R TRα1 using the strip-FRAP technique under physiological T3 levels. Not surprisingly, MED1 coexpression did not change the

intranuclear mobility of either P398R or C392X TRα1. There was no significant difference in mobile and immobile fractions, τ_1, τ_2, C_1, C_2, and $t_{1/2}$ between P398R TRα1 and C392X TRα1 alone and P398R and C392X coexpressed with MED1, and the FRAP profiles of P398R and C392X TRα1 were also not significantly different from wild-type TRα1 (Fig. 5A, 5C, and 5D; $p>0.05$). These results further support our hypothesis that MED1 does not functionally interact with P398R TRα1 and C392X TRα1 under physiological T3 levels.

3.5. MED1 knockout increases the intranuclear mobility of WT TRα1

We previously showed that MED1 overexpression does not impact the intranuclear mobility of wild-type TRα1 at physiological T3 levels; however, the effect of MED1 knockout was not examined (Femia et al., 2020). Since MED1 is a coactivator of TR, we hypothesized that knockout of MED1 would increase the intranuclear mobility of TR, possibly by decreasing the overall residence time of TR on DNA. To test our hypothesis, we transfected $MED1^{+/+}$ and $MED1^{-/-}$ MEFs with wild-type TRα1 and performed strip-FRAP under physiological T3 levels. MED1 knockout significantly decreased the average $t_{1/2}$ of wild-type TRα1 from 1.150 s in $MED1^{+/+}$ MEFs to 0.839 s in $MED1^{-/-}$ MEFs (Table 2; $p<0.05$), supporting our hypothesis. Although no difference in the mobile fraction was found in $MED1^{+/+}$ and $MED1^{-/-}$ MEFs ($p>0.05$), MED1 knockout altered the composition of the mobile fraction. A significantly larger fraction of $MED1^{-/-}$ MEFs was responsible for the short-term recovery (C_1) compared to $MED1^{+/+}$ MEFs ($p<0.01$), while a smaller fraction of $MED1^{-/-}$ MEFs was responsible for the long-term recovery (C_2) compared to $MED1^{+/+}$ MEFs ($p<0.05$) (Table 2). In addition, $MED^{-/-}$ MEFs also had a faster short-term time constant (τ_1) compared to $MED1^{+/+}$ MEFs ($p=0.05$) (Table 2). These results show that MED1 increased the intranuclear mobility of wild-type TRα1, represented by decreased $t_{1/2}$, suggesting that the increase in mobility is potentially caused by a faster short-term recovery time and more proteins undergoing this faster short-term recovery. The faster τ_1 could be explained by the more rapid recovery rate of wild-type TRα1 when not bound to a larger protein, or protein complex like MED1 and the Mediator complex, while the decrease in overall residence time and population of TRα1 on DNA could contribute to the increase in C_1.

3.6. MED1 knockout increases the intranuclear mobility of A263V and P398R TRα1 in the presence of 100 nM T3

Here, we showed that MED1 knockout increases the intranuclear mobility of wild-type TRα1. To further test the interaction between MED1 and TRα1 mutants, we focused on the effect of MED1 knockout on the intranuclear mobility of TRα1 RTH mutants under various T3 levels. We hypothesized that MED1 knockout would not change the intranuclear mobility of A263V, C392X, and P398R TRα1 in the absence of T3 or at physiological (1.2 nM) levels of T3; however, since we showed that increasing the T3 levels to 100 nM partially restores the normal functioning of A263V and P398R TRα1 (see Figs. 3 and 4), we hypothesized that MED1 knockout would increase the intranuclear mobility of A263V and P398R TRα1, but not C392X TRα1 in the presence of T3. We deployed strip-FRAP again to test our hypothesis. Since the most consistent and important parameter for evaluating the effect of MED1 knockout on the mobility of wild-type TRα1 is $t_{1/2,}$ or the time elapsed to recover half of the maximum recovery, we only computed $t_{1/2}$ values for this experiment.

As expected, MED1 knockout did not change the $t_{1/2}$ values of the RTHα mutants, A263V, C392X, and P398R, under physiological T3 levels (Table 3; $p>0.05$). The $t_{1/2}$ values between all mutants and wild-type TRα1 also were not significantly different ($p>0.05$). MED1 knockout also did not change the $t_{1/2}$ values of the TRα1 mutants under T3-depleted conditions (Table 3; $p>0.05$). In contrast, after providing 100 nM of T3, MED1 knockout decreased the average $t_{1/2}$ of A263V TRα1 from 1.3 s in $MED1^{+/+}$ MEFs compared to 0.887 s in $MED1^{-/-}$ MEFs (Table 3; $p<0.05$). We also saw a similar effect in P398R TRα1, where MED1 knockout decreased the average $t_{1/2}$ from 1.453 s in $MED1^{+/+}$ MEFs compared to 1.061 s in $MED1^{-/-}$ MEFs (Table 3; $p<0.05$). However, MED1 knockout did not change the $t_{1/2}$ of C392X TRα1 even in the presence of 100 nM T3 (Table 3; $p>0.05$). Taken together, these data further support our model that A263V and P398R TRα1, comprising less severe forms of RTH mutation, are able to functionally interact with MED1 in the presence of supplemental T3, while C392X TRα1, containing a more severe form of mutation with deletion of the important helix 12, cannot interact with MED1 even in the presence of high levels of T3.

3.7. RTH mutants have altered ligand-dependent transcriptional activity

Since A263V, P398R, and C392X TRα1 have been shown to have reduced T3 sensitivity (Lindl, 2002; Moran et al., 2014; Moran et al., 2017; Tylki-Szymańska et al., 2015; van Gucht et al., 2017), we next sought to ascertain whether these RTHα mutants impacted TR-mediated gene expression in HeLa cells. A firefly luciferase reporter gene under the positive control of a thyroid hormone response element (TRE) was used to examine ligand-dependent transactivation by wild-type TR and the RTH mutants. As expected, wild-type TRα1 significantly induced relative luciferase reporter activity in the presence of 100 nM T3 (Fig. 6, $p=0.001$). A263V TRα1 induced a statistically significant response to T3 ($p=0.015$), but this induction was diminished compared to the response induced by wild-type TRα1 (Fig. 6). P398R TRα1 showed, on average, a comparable induction of reporter gene activity to A263V TRα1; however, there was high inter-sample variability and results were not statistically significant ($p=0.072$). C392X TRα1-mediated transcriptional output was not significantly induced by T3 ($p=0.174$), further indicating the severity of this mutation.

Discussion

We have long been interested in uncovering the interactions between TR and its interaction partners, including exportins, importins, and MED1. We had previously shown that MED1 overexpression does not affect the intranuclear mobility of TRα1 (Femia et al., 2020). Here, we extended our previous research to MED1 knockout MEF cells. We demonstrated that MED1 knockout significantly increases the intranuclear mobility of wild-type TRα1. We also used an improved double exponential fit to analyze the strip-FRAP recovery curve, as suggested by Firmino et al. (2013). This new model allowed us to extract a faster short-term time constant responsible for the immediate recovery of TR, most likely through simple diffusion, and a slower long-term time constant responsible for a gradual recovery, most likely involving dissociation from a protein/protein or protein/DNA complex. The data we acquired from the new model suggest that the increase in mobility of TRα1 is caused in part by a decrease in the short-term time constant, potentially explained by a faster recovery rate

when TRα1 is not associated with a large protein, or protein complex like MED1 and the Mediator complex, leading to a shorter short-term time constant. Other contributing factors to the increased mobility of TRα1 are likely an increase in the TRα1 population responsible for short-term recovery, along with a decrease in the TRα1 population responsible for long-term recovery, potentially explained by a decreased residence time of TRα1 on DNA due to MED1 knockout.

In addition to the interactions between MED1 and wild-type TRα1, we also extended our research to select RTH mutants of TRα1. We demonstrated that MED1 does not modulate the intracellular localization and intranuclear mobility of all TRα1 mutants under physiological levels of T3. When supplemented with 100 nM T3, MED1 overexpression was able to increase the nuclear population of P398R but not C392X TRα1. Similarly, MED1 knockout increased the intranuclear mobility of A263V and C392X TRα1 at these elevated T3 levels. These findings are supported by previous findings that A263V and P398R TRα1 show reduced T3 sensitivity, while C392X TRα1 shows negligible T3 sensitivity (van Gucht et al., 2017). Research has also shown that the dysfunction of A263V TRα1 and the reduced expression of KLF9, a T3 responsive gene mediated by A263V TRα1, is reversed at 100 nM T3 (Moran et al., 2014; Moran et al., 2017). Notably, 100 nM is the same T3 concentration at which we observed functional interactions between MED1 and A263V or P398R TRα1.

Interestingly, we saw a significant number of aggregates in HeLa cells expressing A263V TRα1 alone or expressing both A263V TRα1 and MED1. We demonstrated that A263V TRα1 could also form aggregates with other Mediator complex subunits but not with NCoR1, suggesting that A263V TRα1 interacts with MED1 nonspecifically. Since MED13 knockdown decreases the nuclear population of TR and potentially can interact with TR directly, it will be of interest to investigate the interactions of A263V TRα1 with MED7, MED9, MED10, or MED25, Mediator subunits that do not interact directly with TR but directly bind to MED1 (Fondell, 2012). We also showed that other point mutations near residue 263 in the NES-H6 region of TRα1 contribute to aggregate formation, as we have previously documented in the cancer-associated mutants K74E, A264V and L251P TRα1 (Salomon et al., 2020). Further investigation of RTHα mutations in the NES-H6 region, like M259T, could reveal more insight into TR and MED1 aggregate formation. Our previous research also showed that A225T in the NES-H3 region formed aggregates when expressed in HeLa cells (Salomon et al., 2020). Additional analysis of the interactions between MED1 and D211G, an RTHα mutant in the NES-H3 region, should give more insights into the formation of mutant TR/MED1 co-aggregates.

Of importance, the biochemical data we acquired is in line with clinical records. Since RTHα does not have a signature symptom like goiter in RTHβ and patients have largely normal thyroid function tests, many of the less severe cases of RTHα are left undiagnosed. Our results showed that P398R TRα1 is a less severe form of mutation, in which the normal interaction with MED1 was easily restored at 100 nM T3. This finding matches the clinical record that there is only one known RTHα patient with the P398R mutation. Moreover, the patient did not show severe symptoms and was easily treated with thyroxine supplements (Table 4). Although A263V and A263S are also less severe forms of mutation, both A263V and A263S TRα1 form intracellular aggregates. This aberrant distribution

pattern correlates with more diagnosed cases of RTHα (3 families, 11 cases), but still with less severe and treatable symptoms (Table 4). Our data suggest that C392X is a severe form of mutation, since providing 100 nM of T3 did not restore the normal interaction between C392X TRα1 and MED1. This finding is reflected in the clinical record, where a large range of severe symptoms are associated with the C392X mutation that are not treatable by simply providing thyroxine supplements to the patients (Table 4). It will be of interest to examine how other severe RTH mutations, such as L274P and other helix 12 deletion mutations (C380fsX8, C380fsX9, A382fsX7, E395X, and F397fsX10) (Moran et al., 2017), change the interactions between mutant TR and MED1. Recent research has also discovered mutations in the Hinge domain, where the RTH pathology was attributed to the increased inhibitory function of TRα2, a TR variant that does not bind T3 (Paisdzior et al., 2021). Investigating the interactions between such TRα1 mutants (I170V and E173G) and MED1 will further enhance our understanding of TRα1-MED1 interactions and the biochemical basis of RTHα.

Acknowledgments

This work was supported by Grant 2R15DK058028 from the National Institutes of Health (to L.A.A.).

References

Allison LA, 2021. Getting there: Thyroid hormone receptor intracellular trafficking. J. Biol. Chem 296, 100677. 10.1016/j.jbc.2021.100677 [PubMed: 33887322]

Bassett JH, Williams GR, 2003. The molecular actions of thyroid hormone in bone. Trends Endocrinol. Metab 14, 356–364. 10.1016/s1043-2760(03)00144-9 [PubMed: 14516933]

Bochukova E, Schoenmakers N, Agostini M, Schoenmakers E, Rajanayagam O, Keogh JM, Henning E, Reinemund J, Gevers E, Sarri M, Downes K, Offiah A, Albanese A, Halsall D, Schwabe JW, Bain M, Lindley K, Muntoni F, Vargha-Khadem F, Dattani M, Farooqi IS, Gurnell M, Chatterjee K, 2012. A mutation in the thyroid hormone receptor alpha gene. N. Engl. J. Med 366, 243–249. 10.1056/NEJMoa1110296 [PubMed: 22168587]

Boija A, Klein IA, Sabari BR, Dall'Agnese A, Coffey EL, Zamudio AV, Li CH, Shrinivas K, Manteiga JC, Hannett NM, Abraham BJ, Afeyan LK, Guo YE, Rimel JK, Fant CB, Schuijers J, Lee TI, Taatjes DJ, Young RA, 2018. Transcription Factors Activate Genes through the Phase-Separation Capacity of Their Activation Domains. Cell 175, 1842–1855.e16. 10.1016/j.cell.2018.10.042 [PubMed: 30449618]

Brent GA, 2012. Mechanisms of thyroid hormone action. J. Clin. Invest 122, 3035–3043. 10.1172/JCI60047 [PubMed: 22945636]

Bunn CF, Neidig JA, Freidinger KE, Stankiewicz TA, Weaver BS, McGrew J, Allison LA, 2001. Nucleocytoplasmic shuttling of the thyroid hormone receptor alpha. Mol. Endocrinol 15, 512–533. 10.1210/mend.15.4.0619 [PubMed: 11266504]

Chávez E, Franco M, Reyes-Vivas H, Zazueta C, Ramírez J, Carrillo R, 1998. Hypothyroidism renders liver mitochondria resistant to the opening of membrane permeability transition pore. Biochim. Biophys. Acta 1407, 243–248. 10.1016/s0925-4439(98)00048-9 [PubMed: 9748606]

Chen XY, Liu Y, Liu JH, Qin XS, 2019. An analysis of GNAS and THRA gene mutations in children with congenital hypothyroidism. Zhongguo Dangdai Erke Zazhi 21, 680–684. 10.7499/j.issn.1008-8830.2019.07.012 [PubMed: 31315768]

Contreras-Jurado C, García-Serrano L, Martínez-Fernández M, Ruiz-Llorente L, Paramio JM, Aranda A, 2014. Impaired hair growth and wound healing in mice lacking thyroid hormone receptors. PLoS One 9, e108137. 10.1371/journal.pone.0108137 [PubMed: 25254665]

Demir K, van Gucht AL, Büyükinan M, Çatlı G, Ayhan Y, Baş VN, Dündar B, Özkan B, Meima ME, Visser WE, Peeters RP, Visser TJ, 2016. Diverse Genotypes and Phenotypes of Three Novel

Thyroid Hormone Receptor-α Mutations. J. Clin. Endocrinol. Metab 101, 2945–2954. 10.1210/jc.2016-1404 [PubMed: 27144938]

Dinda S, Sanchez A, Moudgil V, 2002. Estrogen-like effects of thyroid hormone on the regulation of tumor suppressor proteins, p53 and retinoblastoma, in breast cancer cells. Oncogene 21, 761–768. 10.1038/sj.onc.1205136 [PubMed: 11850804]

Femia MR, Evans RM, Zhang J, Sun X, Lebegue CJ, Roggero VR, Allison LA, 2020. Mediator subunit MED1 modulates intranuclear dynamics of the thyroid hormone receptor. J. Cell. Biochem 121, 2909–2926. 10.1002/jcb.29532 [PubMed: 31692077]

Figueira AC, Saidemberg DM, Souza PC, Martínez L, Scanlan TS, Baxter JD, Skaf MS, Palma MS, Webb P, Polikarpov I, 2011. Analysis of agonist and antagonist effects on thyroid hormone receptor conformation by hydrogen/deuterium exchange. Mol. Endocrinol 25, 15–31. 10.1210/me.2010-0202 [PubMed: 21106879]

Firmino J, Tinevez JY, Knust E, 2013. Crumbs affects protein dynamics in anterior regions of the developing Drosophila embryo. PloS one 8, e58839. 10.1371/journal.pone.0058839 [PubMed: 23555600]

Fondell JD, 2013. The Mediator complex in thyroid hormone receptor action. Biochim. Biophys. Acta 1830, 3867–3875. 10.1016/j.bbagen.2012.02.012 [PubMed: 22402254]

Fozzatti L, Kim DW, Park JW, Willingham MC, Hollenberg AN, & Cheng S-Y, 2013. Nuclear receptor corepressor (NCOR1) regulates in vivo actions of a mutated thyroid hormone receptor α. Proc. Natl. Acad. Sci. USA 110, 7850–7855. 10.1073/pnas.1222334110 [PubMed: 23610395]

Furman AE, Dumitrescu AM, Refetoff S, Weiss RE, 2021. Early Diagnosis and Treatment of an Infant with a Novel Thyroid Hormone Receptor α Gene (pC380SfsX9) Mutation. Thyroid 31, 1003–1005. 10.1089/thy.2020.0695 [PubMed: 33198587]

González-Pérez V, Schmierer B, Hill CS, Sear RP, 2011. Studying Smad2 intranuclear diffusion dynamics by mathematical modelling of FRAP experiments. Integr. Biol 3, 197–207. 10.1039/c0ib00098a

Hollenberg AN, Monden T, Madura JP, Lee K, Wondisford FE, 1996. Function of nuclear co-repressor protein on thyroid hormone response elements is regulated by the receptor A/B domain. J. Biol. Chem 271, 28516–28520. 10.1074/jbc.271.45.28516 [PubMed: 8910480]

Hörlein AJ, Näär AM, Heinzel T, Torchia J, Gloss B, Kurokawa R, Ryan A, Kamei Y, Söderström M, Glass CK, 1995. Ligand-independent repression by the thyroid hormone receptor mediated by a nuclear receptor co-repressor. Nature 377, 397–404. 10.1038/377397a0 [PubMed: 7566114]

Ito M, Yuan CX, Okano HJ, Darnell RB, Roeder RG, 2000. Involvement of the TRAP220 component of the TRAP/SMCC coactivator complex in embryonic development and thyroid hormone action. Mol. Cell 5, 683–693. 10.1016/s1097-2765(00)80247-6 [PubMed: 10882104]

Jin F, Claessens F, Fondell JD, 2012. Regulation of androgen receptor-dependent transcription by coactivator MED1 is mediated through a newly discovered noncanonical binding motif. J. Biol. Chem 287, 858–870. 10.1074/jbc.M111.304519 [PubMed: 22102282]

Kalikiri MK, Mamidala MP, Rao AN, Rajesh V, 2017. Analysis and functional characterization of sequence variations in ligand binding domain of thyroid hormone receptors in autism spectrum disorder (ASD) patients. Autism Res. 10 1919–1928. 10.1002/aur.1838 [PubMed: 28856816]

Koenig RJ, 1998. Thyroid hormone receptor coactivators and corepressors. Thyroid 8, 703–713. 10.1089/thy.1998.8.703 [PubMed: 9737367]

Korkmaz O, Ozen S, Ozdemir TR, Goksen D, Darcan S, 2019. A novel thyroid hormone receptor alpha gene mutation, clinic characteristics, and follow-up findings in a patient with thyroid hormone resistance. Hormones 18, 223–227. 10.1007/s42000-019-00094-9 [PubMed: 30747412]

Laudet V, Gronemeyer H, 2002. The Nuclear Receptor Factsbook, first ed. Academic Press, Massachusetts.

le Maire A, Bouhours-Nouet N, Soamalala J, Mirebeau-Prunier D, Paloni M, Guee L, Heron D, Mignot C, Illouz F, Joubert F, Briet C, Rodien P, Bourguet W, Flamant F, Guyot R, 2020. Two Novel Cases of Resistance to Thyroid Hormone Due to THRA Mutation. Thyroid 30, 1217–1221. 10.1089/thy.2019.0602 [PubMed: 32204686]

Lindl T (2002). Zell- und Gewebekultur Einführung in die Grundlagen Sowie ausgewählte methoden und Anwendungen. Akademie Verlag, Germany.

Liu G, Sprenger C, Wu PJ, Sun S, Uo T, Haugk K, Epilepsia KS, Plymate S, 2015. MED1 mediates androgen receptor splice variant induced gene expression in the absence of ligand. Oncotarget 6, 288–304. 10.18632/oncotarget.2672 [PubMed: 25481872]

Mavinakere MS, Powers JM, Subramanian KS, Roggero VR, Allison LA, 2012. Multiple novel signals mediate thyroid hormone receptor nuclear import and export. J. Biol. Chem 287, 31280–31297. 10.1074/jbc.M112.397745 [PubMed: 22815488]

Moran C, Agostini M, McGowan A, Schoenmakers E, Fairall L, Lyons G, Rajanayagam O, Watson L, Offiah A, Barton J, Price S, Schwabe J, Chatterjee K, 2017. Contrasting Phenotypes in Resistance to Thyroid Hormone Alpha Correlate with Divergent Properties of Thyroid Hormone Receptor α1 Mutant Proteins. Thyroid 27, 973–982. 10.1089/thy.2017.0157 [PubMed: 28471274]

Moran C, Agostini M, Visser WE, Schoenmakers E, Schoenmakers N, Offiah AC, Poole K, Rajanayagam O, Lyons G, Halsall D, Gurnell M, Chrysis D, Efthymiadou A, Buchanan C, Aylwin S, Chatterjee KK, 2014. Resistance to thyroid hormone caused by a mutation in thyroid hormone receptor (TR)α1 and TRα2: clinical, biochemical, and genetic analyses of three related patients. Lancet Diabetes Endocrinol. 2, 619–626. 10.1016/S2213-8587(14)70111-1 [PubMed: 24969835]

Moran C, Schoenmakers N, Agostini M, Schoenmakers E, Offiah A, Kydd A, Kahaly G, Mohr-Kahaly S, Rajanayagam O, Lyons G, Wareham N, Halsall D, Dattani M, Hughes S, Gurnell M, Park SM, Chatterjee K, 2013. An adult female with resistance to thyroid hormone mediated by defective thyroid hormone receptor α. J. Clin. Endocrinol. Metab 98, 4254–4261. 10.1210/jc.2013-2215 [PubMed: 23940126]

Moras D, Gronemeyer H, 1998. The nuclear receptor ligand-binding domain: structure and function. Curr. Opin. Cell Biol 10, 384–391. 10.1016/s0955-0674(98)80015-x [PubMed: 9640540]

Mullur R, Liu YY, Brent GA, 2014. Thyroid hormone regulation of metabolism. Physiol. Rev 94, 355–382. 10.1152/physrev.00030.2013 [PubMed: 24692351]

Nagulapalli M, Maji S, Dwivedi N, Dahiya P, Thakur JK, 2016. Evolution of disorder in Mediator complex and its functional relevance. Nucleic Acids Res. 44, 1591–1612. 10.1093/nar/gkv1135 [PubMed: 26590257]

Ortiga-Carvalho TM, Sidhaye AR, Wondisford FE, 2014. Thyroid hormone receptors and resistance to thyroid hormone disorders. Nature reviews. Endocrinology 10, 582–591. 10.1038/nrendo.2014.143 [PubMed: 25135573]

Paisdzior S, Knierim E, Kleinau G, Biebermann H, Krude H, Straussberg R, Schuelke M, 2021. A New Mechanism in THRA Resistance: The First Disease-Associated Variant Leading to an Increased Inhibitory Function of THRA2. Int. J. Mol. Sci 22, 5338. 10.3390/ijms22105338 [PubMed: 34069457]

Palacio M, Taatjes DJ, 2022. Merging Established Mechanisms with New Insights: Condensates, Hubs, and the Regulation of RNA Polymerase II Transcription. J. Mol. Biol 434, 167216. 10.1016/j.jmb.2021.167216 [PubMed: 34474085]

Pascual A, Aranda A, 2013. Thyroid hormone receptors, cell growth and differentiation. Biochim. Biophys. Acta 1830, 3908–3916. 10.1016/j.bbagen.2012.03.012 [PubMed: 22484490]

Phair RD, Gorski SA, Misteli T, 2004. Measurement of dynamic protein binding to chromatin in vivo, using photobleaching microscopy. Methods Enzymol. 375, 393–414. 10.1016/s0076-6879(03)75025-3 [PubMed: 14870680]

Préau L, Fini JB, Morvan-Dubois G, Demeneix B, 2015. Thyroid hormone signaling during early neurogenesis and its significance as a vulnerable window for endocrine disruption. Biochim. Biophys. Acta 1849, 112–121. 10.1016/j.bbagrm.2014.06.015 [PubMed: 24980696]

Puzianowska-Kuznicka M, Pietrzak M, Turowska O, Nauman A, 2006. Thyroid hormones and their receptors in the regulation of cell proliferation. Acta Biochim. Pol 53, 641–650. [PubMed: 17115080]

Qi JS, Yuan Y, Desai-Yajnik V, Samuels HH, 1999. Regulation of the mdm2 oncogene by thyroid hormone receptor. Mol. Cell. Biol 19, 864–872. 10.1128/MCB.19.1.864 [PubMed: 9858609]

Sabari BR, Dall'Agnese A, Boija A, Klein IA, Coffey EL, Shrinivas K, Abraham BJ, Hannett NM, Zamudio AV, Manteiga JC, Li CH, Guo YE, Day DS, Schuijers J, Vasile E, Malik S, Hnisz D, Lee TI, Cisse II, Roeder RG, Sharp PA, Chakraborty AK, Young RA, 2018. Coactivator

condensation at super-enhancers links phase separation and gene control. Science 361, eaar3958. 10.1126/science.aar3958 [PubMed: 29930091]

Salomon MS, Malapati SH, O' Dwyer J, Silva CL, Williams CC, Barbeau MC, Yip D, Punzalan P, Nagle VL, Hinton SD, Roggero VR, Allison LA, 2020. Mislocalization of Cancer-associated Thyroid Hormone Receptor Mutants. Nucl. Recept. Res 2020.

Sap J, Muñoz A, Damm K, Goldberg Y, Ghysdael J, Leutz A, Beug H, Vennström B, 1986. The c-erb-A protein is a high-affinity receptor for thyroid hormone. Nature 324, 635–640. 10.1038/324635a0 [PubMed: 2879242]

Shi Y, Chen J, Zeng W-J, Li M, Zhao W, Zhang X-D, Yao J, 2021. Formation of nuclear condensates by the mediator complex subunit med15 in mammalian cells. BMC Biol. 19. 10.1186/s12915-021-01178-y

Singh BK, Yen PM, 2017. A clinician's guide to understanding resistance to thyroid hormone due to receptor mutations in the TRα and TRβ isoforms. Clin. Diabetes Endocrinol 3, 8. 10.1186/s40842-017-0046-z [PubMed: 28932413]

Soutourina J, 2018. Transcription regulation by the Mediator complex. Nature reviews. Nat. Rev. Mol. Cell Biol 19, 262–274. 10.1038/nrm.2017.115 [PubMed: 29209056]

Stepien BK, Huttner WB, 2019. Transport, Metabolism, and Function of Thyroid Hormones in the Developing Mammalian Brain. Front. Endocrinol 10, 209. 10.3389/fendo.2019.00209

Sun H, Cao L, Zheng R, Xie S, Liu C, 2020. Update on resistance to thyroid hormone syndromeβ. Ital. J. Pediatr 46, 168. 10.1186/s13052-020-00929-x [PubMed: 33176840]

Sun H, Wu H, Xie R, Wang F, Chen T, Chen X, Wang X, Flamant F, Chen L, 2019. New case of thyroid hormone resistance α caused by a mutation of Thra/TRA1. J. Endocr. Soc 3, 665–669. 10.1210/js.2019-00011 [PubMed: 30842990]

Tylki-Szymańska A, Acuna-Hidalgo R, Krajewska-Walasek M, Lecka-Ambroziak A, Steehouwer M, Gilissen C, Brunner HG, Jurecka A, Różdżyńska-Świątkowska A, Hoischen A, Chrzanowska KH, 2015. Thyroid hormone resistance syndrome due to mutations in the thyroid hormone receptor α gene (THRA). J. Med. Genet 52, 312–316. 10.1136/jmedgenet-2014-102936 [PubMed: 25670821]

Umesono K, Evans RM, 1989. Determinants of target gene specificity for steroid/thyroid hormone receptors. Cell 57, 1139–1146. 10.1016/0092-8674(89)90051-2 [PubMed: 2500251]

van Gucht A, Meima ME, Moran C, Agostini M, Tylki-Szymanska A, Krajewska MW, Chrzanowska K, Efthymiadou A, Chrysis D, Demir K, Visser WE, Visser TJ, Chatterjee K, van Dijk TB, Peeters RP, 2017. Anemia in Patients With Resistance to Thyroid Hormone α: A Role for Thyroid Hormone Receptor α in Human Erythropoiesis. J. Clin. Endocrinol. Metab 102, 3517–3525. 10.1210/jc.2017-00840 [PubMed: 28911146]

van Gucht AL, Meima ME, Zwaveling-Soonawala N, Visser WE, Fliers E, Wennink JM, Henny C, Visser TJ, Peeters RP, van Trotsenburg AS, 2016. Resistance to Thyroid Hormone Alpha in an 18-Month-Old Girl: Clinical, Therapeutic, and Molecular Characteristics. Thyroid 26, 338–346. 10.1089/thy.2015.0463 [PubMed: 26782358]

van Gucht AL, Moran C, Meima ME, Visser WE, Chatterjee K, Visser TJ, Peeters RP, 2017. Resistance to Thyroid Hormone due to Heterozygous Mutations in Thyroid Hormone Receptor Alpha. Curr. Top. Dev. Biol 125, 337–355. 10.1016/bs.ctdb.2017.02.001 [PubMed: 28527577]

van Mullem A, van Heerebeek R, Chrysis D, Visser E, Medici M, Andrikoula M, Tsatsoulis A, Peeters R, Visser TJ, 2012. Clinical phenotype and mutant TRα1. N. Engl. J. Med 366, 1451–1453. 10.1056/NEJMc1113940

Weinberger C, Thompson CC, Ong ES, Lebo R, Gruol DJ, Evans RM, 1986. The c-erb-A gene encodes a thyroid hormone receptor. Nature 324, 641–646. 10.1038/324641a0 [PubMed: 2879243]

Weiss RE, Refetoff S, 2000. Resistance to Thyroid Hormone. Rev. Endocr. Metab. Disord 1, 97–108. 10.1023/a:1010072605757 [PubMed: 11704998]

Williams GR, 2009. Actions of thyroid hormones in bone. Endokrynol. Pol 60, 380–388. [PubMed: 19885809]

Wojcicka A, Bassett JH, Williams GR, 2013. Mechanisms of action of thyroid hormones in the skeleton. Biochim. Biophys. Acta 1830, 3979–3986. 10.1016/j.bbagen.2012.05.005 [PubMed: 22634735]

Yoh SM, Privalsky ML, 2001. Transcriptional repression by thyroid hormone receptors. A role for receptor homodimers in the recruitment of SMRT corepressor. J. Biol. Chem 276, 16857–16867. 10.1074/jbc.M010022200 [PubMed: 11278601]

Yuan CX, Ito M, Fondell JD, Fu ZY, Roeder RG, 1998. The TRAP220 component of a thyroid hormone receptor- associated protein (TRAP) coactivator complex interacts directly with nuclear receptors in a ligand-dependent fashion. Proc. Natl. Acad. Sci. U. S. A 95, 7939–7944. 10.1073/pnas.95.14.7939 [PubMed: 9653119]

Yuen RK, Thiruvahindrapuram B, Merico D, Walker S, Tammimies K, Hoang N, Chrysler C, Nalpathamkalam T, Pellecchia G, Liu Y, Gazzellone MJ, D'Abate L, Deneault E, Howe JL, Liu RS, Thompson A, Zarrei M, Uddin M, Marshall CR, Ring RH, Zwaigenbaum L, Ray PN, Weksberg R, Carter MT, Fernandez BA, Roberts W, Szatmari P, Scherer SW, 2015. Whole-genome sequencing of quartet families with autism spectrum disorder. Nat. Med 21, 185–191. 10.1038/nm.3792 [PubMed: 25621899]

Zhang J, Roggero VR, Allison LA, 2018. Nuclear import and export of the thyroid hormone receptor. Vitam. Horm 106, 45–66. 10.1016/bs.vh.2017.04.002 [PubMed: 29407444]

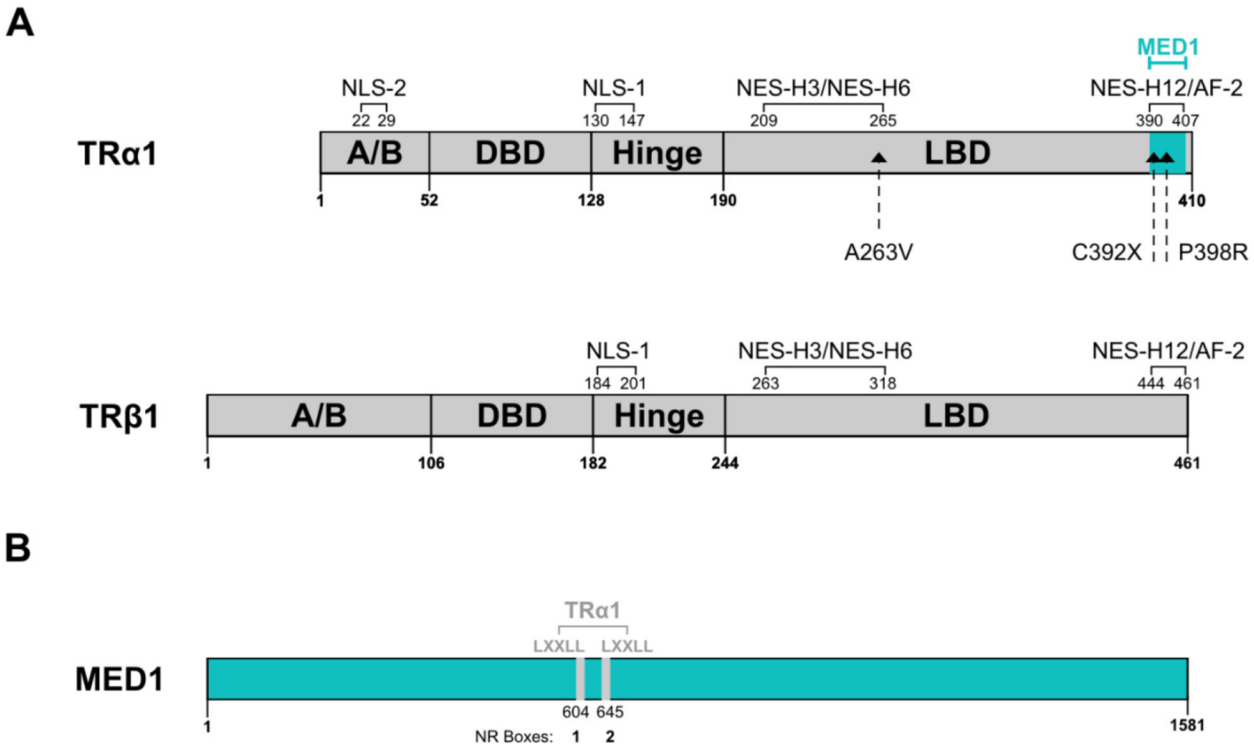

Fig. 1.

Functional domains of TRα1, TRβ1, and MED1. (A) Domains for TRα1 and TRβ1. TRβ1 has a longer A/B domain than TRα1. The other three domains are conserved between TRα1 and TRβ1. Several NLS and NES motifs have been identified in both TRα1 and TRβ1. MED1 binds to helix 12 of TRα1. RTH mutations selected for this research (A263V, C392X, and P398R) are marked on TRα1. (B) Schematic of MED1. MED1 interacts with TR using two conserved NR boxes with LXXLL motifs located at amino acids 604 and 645. A/B, A/B domain; DBD, DNA binding domain; Hinge, hinge domain; LBD, ligand binding domain; NLS, nuclear localization signal; NES, nuclear export signal; H3, helix 3; H6, helix 6; H12, helix 12; AF-2, activation function 2 domain; NR box, nuclear receptor box.

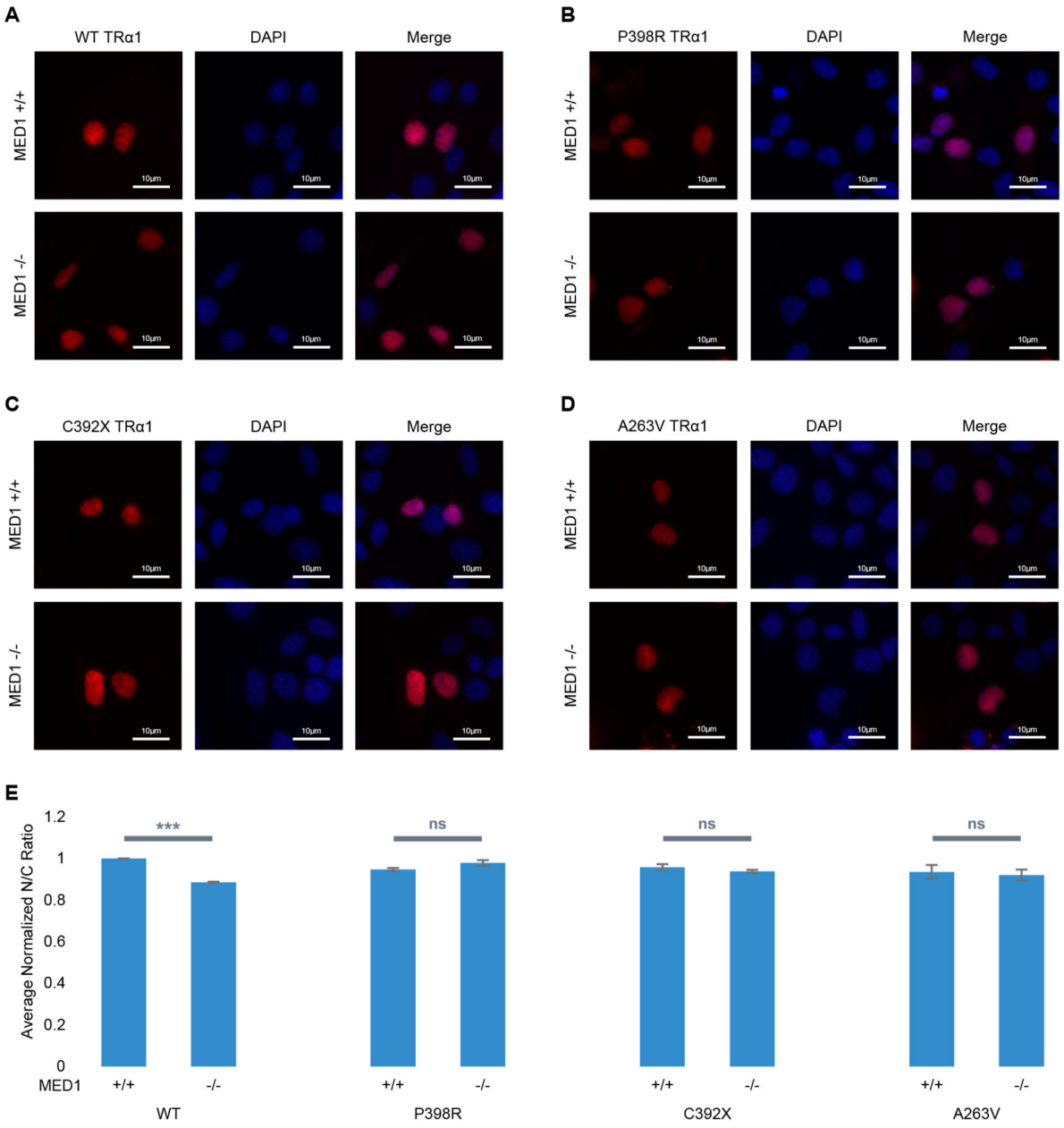

Fig. 2.

Knockout of MED1 decreases the nuclear population of wild-type (WT) TRα1. mCherry tagged WT TRα1 (A), P398R TRα1 (B), C392X TRα1 (C), and A263V TRα1 (D) expression plasmids were transfected into $MED1^{+/+}$ and $MED1^{-/-}$ MEFs. Cells were analyzed by fluorescence microscopy 24 hours post-transfection. Representative images are shown. Scale bar = 10 μm. (E) Bars represent the average normalized N/C ratios, calculated by normalizing the mutant N/C ratio to WT ($MED1^{+/+}$). Error bars indicate +/− SEM (n=3 biologically independent replicates, with 60 cells per replicate). *** $p<0.001$, ns $p>0.05$.

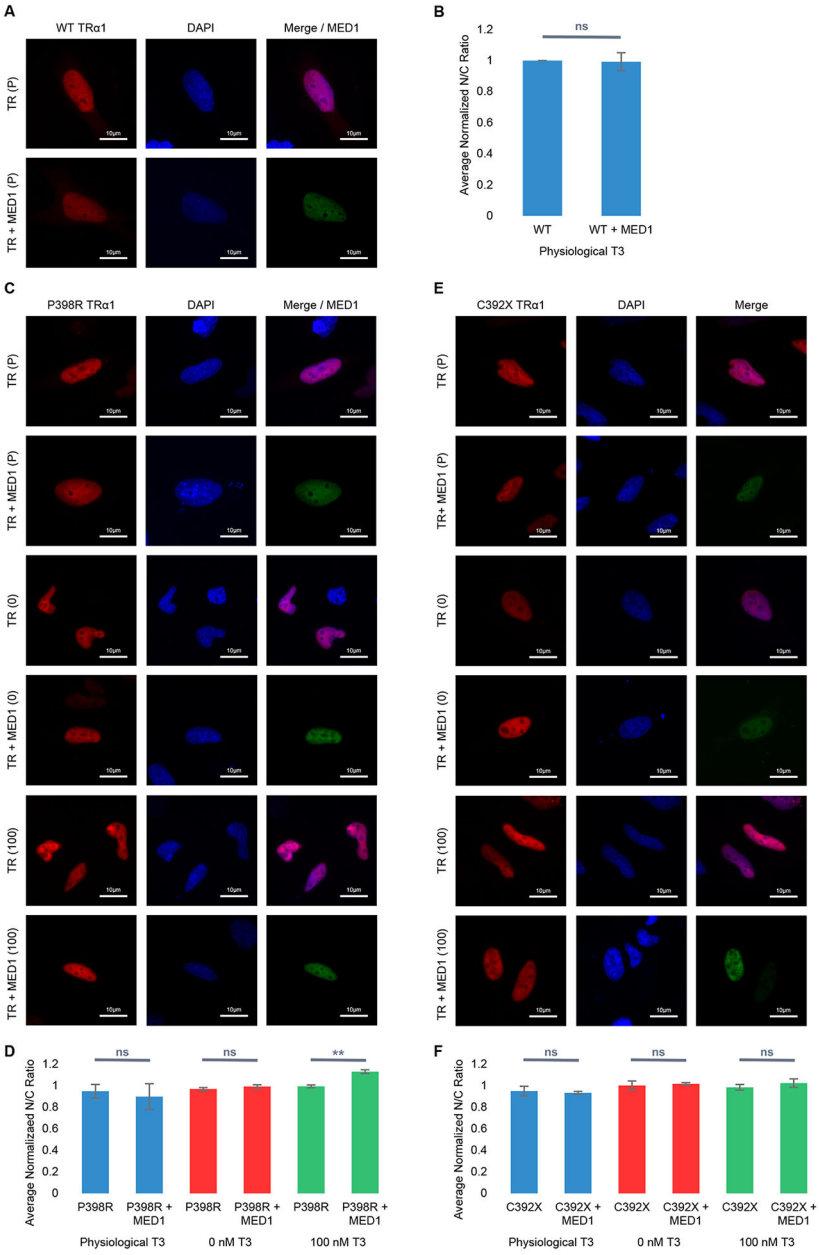

Fig. 3.

MED1 overexpression increases the N/C ratio of P398R TRα1 at elevated T3 levels. mCherry-tagged WT TRα1 (A), P398RX TRα1 (C), and C392X TRα1 (E) expression plasmids were either single transfected or cotransfected with GFP-MED1 into HeLa cells at physiological, 0 nM, or 100 nM T3 levels. Cells were analyzed by fluorescence microscopy 24 hours post-transfection. Representative images are shown. Scale bars = 10 μm. Average normalized N/C ratios were calculated by normalizing the mutant N/C ratio to WT. Bars represent the average normalized N/C ratio of WT TRα1 (B), P398R TRα1 (D), or C392X TRα1 (F) under different T3 levels. Error bars indicate +/− SEM (n=3 biologically independent replicates, with 60 cells per replicate). ** $p<0.01$, ns $p>0.05$. P: Physiological T3; 0: 0 nM T3; 100: 100 nM T3.

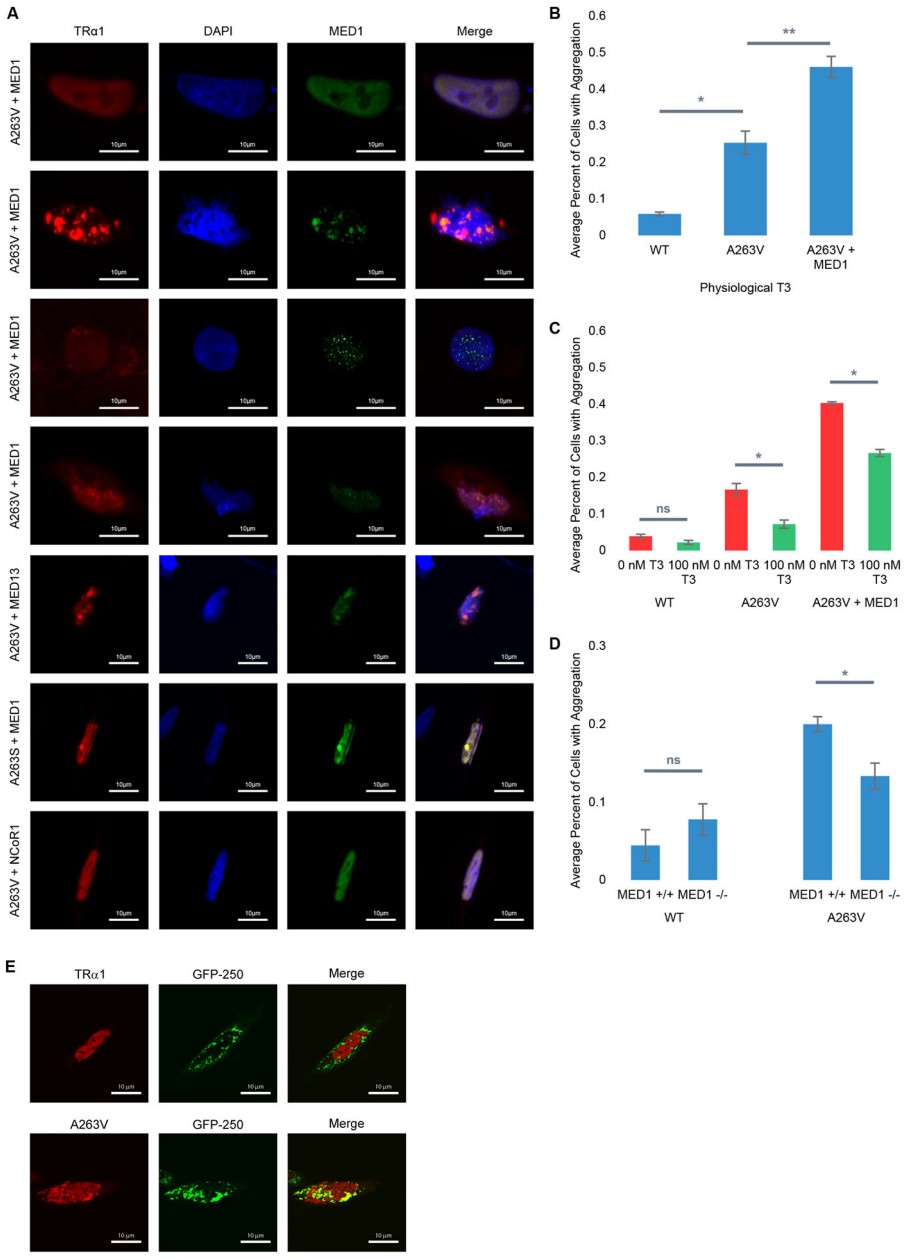

Fig. 4.

MED1 overexpression increases the percentage of A263V-expressing cells with aggregates, while MED1 knockout and T3 supplementation decrease the percentage of cells with aggregates. mCherry-tagged WT, A263V, and A263S TRα1 expression plasmids were either single-transfected or cotransfected with GFP-MED1 or GFP-MED13 into HeLa cells, $MED1^{+/+}$ MEFs, and $MED^{-/-}$ MEFs, as indicated. Cells were analyzed by fluorescence microscopy 24 hours post-transfection. (A) Representative images are shown for different transfection schemes. Scale bar = 10 μm. (B) Bars represent the average percent of cells with TR aggregates for each transfection scheme under physiological levels of T3. (C) Bars represent the average percent of cells with TR aggregates for each transfection scheme under depleted or elevated levels of T3. The presence or absence of aggregates was assessed

qualitatively by scoring cells as having “no aggregation” (homogeneous distribution of TR without any bright fluorescent foci) or having “aggregation” (bright fluorescent foci of TR, ranging from speckles to larger aggregates). (D) Bars represent the average percent of cells with TR aggregates for $MED1^{+/+}$ or $MED1^{-/-}$ MEFs under physiological levels of T3. Error bars indicate +/− SEM (n=3 biologically independent replicates, with 60 cells per replicate). *$p<0.05$, **$p<0.01$, ns $p>0.05$). (E) HeLa cells cotransfected with the aggresome marker GFP-250 and either wild-type or A263V TRα1 were analyzed for colocalization of aggregates and aggresomes by confocal microscopy.

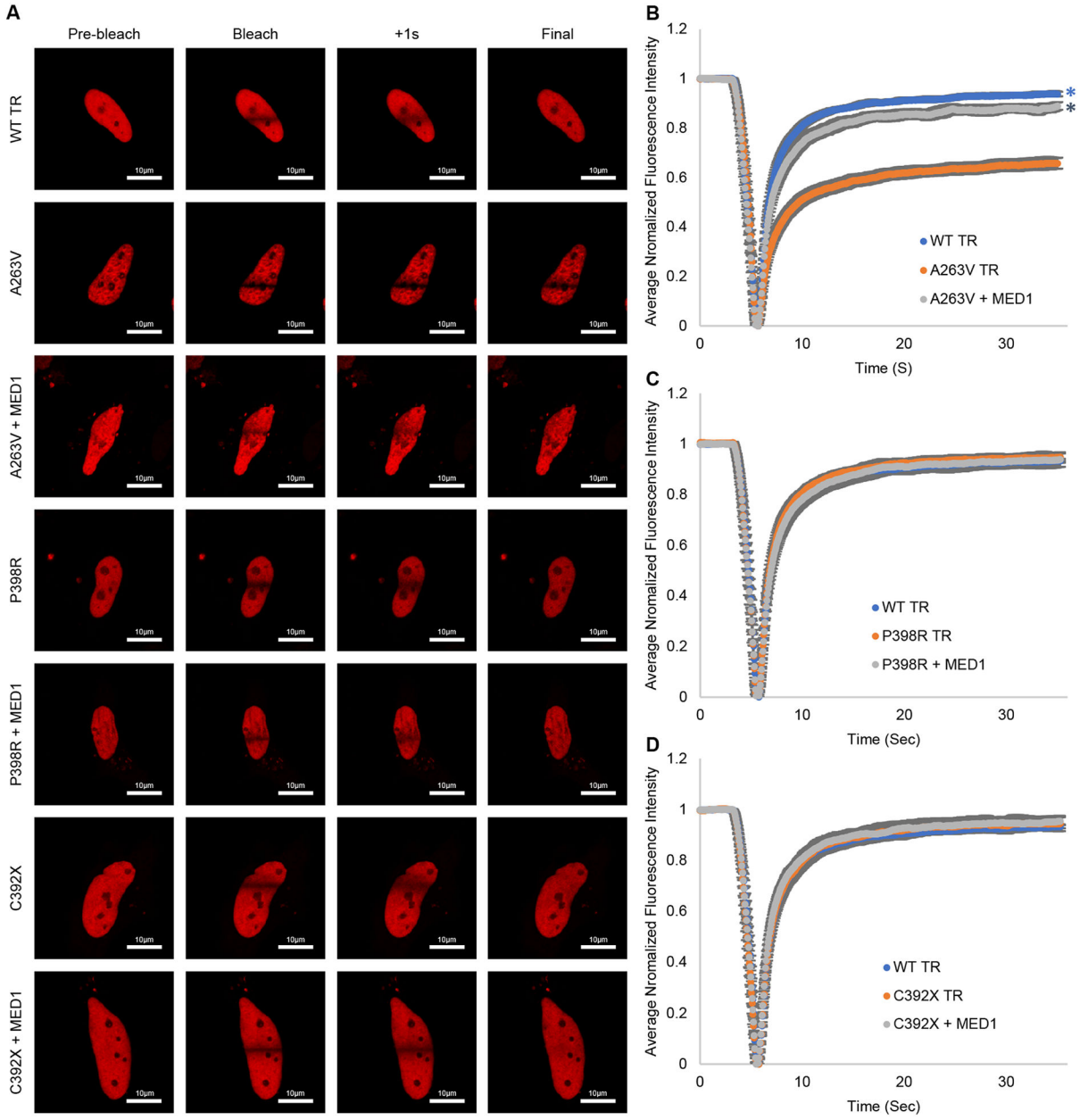

Fig. 5.

Overexpression of MED1 rescues the decreased intranuclear mobility of A263V TRα1. mCherry tagged WT, A263V, P398R, and C392X TRα1 expression plasmids were either single-transfected or cotransfected with GFP-MED1 into HeLa cells. Strip-FRAP was performed 24 h post transfection on 20 nuclei with a stimulation bleaching line near the middle of each nucleus. (A) Representative nuclei prior to bleach (pre-bleach), directly after bleaching terminated (bleach), 1 s post-bleach (+1s), and at the end of the recovery (final). Graphs represent the average normalized fluorescence intensity for each time point for A263V (B), P398R (C), and C392X TRα1 (D). Error bars indicate +/− SEM (n=3 biologically independent replicates, with 20 nuclei per replicate). * $p<0.05$.

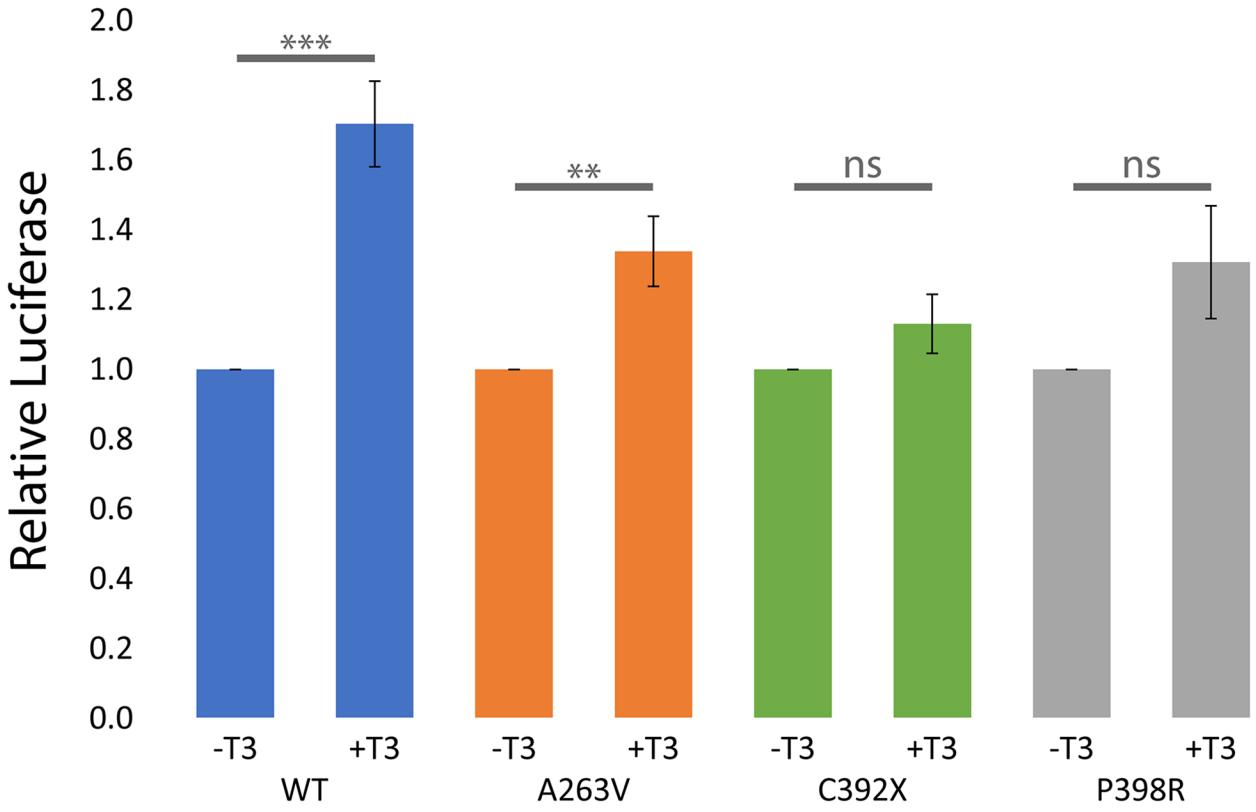

Fig. 6.

TR-mediated T3-dependent reporter gene transactivation is diminished in RTH mutants. (A) HeLa cells were cotransfected with expression plasmids for wild-type (WT) GFP-TRα1 and the RTH mutants, as indicated, TRE (DR+4)-firefly luciferase reporter, and Renilla luciferase internal control, in the presence or absence of 100 nM T3. Data are presented as relative firefly/Renilla luciferase activity (Relative Luciferase) normalized to -T3. Error bars indicate ± SEM (n=3 biologically independent replicates of 8 wells per treatment). ***p<0.001, **p<0.01, ns p>0.05.

Table 1.

Intranuclear FRAP profile for wild-type (WT) and A263V TRα1 in HeLa cells under physiological T3 levels.[a]

	WT **WT vs A263V**	**A263V** **A263V ± MED1**	**A263V + MED1** **WT vs A263V + MED1**
Mobile Fraction	0.938 ± 0.010 **p = 0.0002** *	0.665 ± 0.028 **p = 0.0003** *	0.882 ± 0.020 **p = 0.044** *
Immobile Fraction	0.062 ± 0.010 **p = 0.0002** *	0.335 ± 0.028 **p = 0.0003** *	0.118 ± 0.020 **p = 0.044** *
τ_1 (s)	1.154 ± 0.013 p = 0.589	1.182 ± 0.047 p = 0.168	1.101 ± 0.021 p = 0.071
τ_2 (s)	7.142 ± 0.383 p = 0.189	8.977 ± 1.139 p = 0.063	6.086 ± 0.511 p = 0.140
C_1	0.742 ± 0.010 **p = 0.0003** *	0.431 ± 0.032 **p = 0.002** *	0.617 ± 0.028 **p = 0.009** *
C_2	0.196 ± 0.007 **p = 0.037** *	0.234 ± 0.012 p = 0.178	0.265 ± 0.016 **p = 0.010** *
$t_{1/2}$ (s)	1.045 ± 0.012 **p = 0.0002** *	1.403 ± 0.035 **p = 0.0005** *	1.126 ± 0.034 p = 0.072

[a] τ_1 and τ_2 are the time constants for short-term and long-term recovery, respectively. C_1 and C_2 are the fractions of proteins responsible for the short-term and long-term recovery process, respectively. $t_{1/2}$ represents the time taken to reach 50% of maximum recovery.

* $p<0.05$.

Table 2.

Intranuclear FRAP profile for wild-type (WT) TRα1 in MED1$^{+/+}$ and MED1$^{-/-}$ MEFs under physiological T3 levels.[a]

	MED1$^{+/+}$	**MED1$^{-/-}$**	**p value**
Mobile Fraction	0.943 ± 0.005	0.951 ± 0.002	0.672
Immobile Fraction	0.057 ± 0.005	0.049 ± 0.002	0.672
τ_1 (s)	1.036 ± 0.003	0.915 ± 0.009	**0.050**[*]
τ_2 (s)	5.876 ± 0.199	5.222 ± 0.124	0.475
C_1	0.613 ± 0.004	0.741 ± 0.006	**0.009**[*]
C_2	0.330 ± 0.008	0.211 ± 0.007	**0.029**[*]
$t_{1/2}$ (s)	1.150 ± 0.006	0.839 ± 0.015	**0.015**[*]

[a] τ_1 and τ_2 are the time constants for short-term and long-term recovery, respectively. C_1 and C_2 are the fractions of proteins responsible for the short-term and long-term recovery process, respectively. $t_{1/2}$ represents the time taken to reach 50% of maximum recovery.

[*] $p<0.05$.

Table 3.

$t_{1/2}$ for wild-type, A623V, C392X, and P398R TRα1 under different T3 levels determined by FRAP.

T3 Treatment	TRα1 Variant	MED1$^{+/+}$	MED1$^{-/-}$	p value
Physiological	WT	1.150 ± 0.006	0.839 ± 0.015	**0.015** *
	A263V	0.988 ± 0.028	0.916 ± 0.025	0.608
	C392X	1.102 ± 0.014	0.966 ± 0.004	0.096
	P398R	0.992 ± 0.022	0.962 ± 0.030	0.823
0 nM	A263V	1.402 ± 0.103	1.235 ± 0.016	0.688
	C392X	2.092 ± 0.162	1.162 ± 0.022	0.097
	P398R	1.779 ± 0.059	1.779 ± 0.061	0.999
100 nM	A263V	1.300 ± 0.024	0.887 ± 0.012	**0.023** *
	C392X	1.867 ± 0.047	1.439 ± 0.062	0.192
	P398R	1.453 ± 0.030	1.061 ± 0.017	**0.036** *

* $p<0.05$.

Table 4.

Clinical records for RTH patients with A263V, C392X, and P398R TRα1 mutations.

Mutation	**A263V**	**A263S**	**C392X**	**P398R**
# of Families	2	1	2	1
# of Cases *	3 + 1	7	1 + 1	1
Countries	UK	Turkey	China; Poland	Poland
Selected Patient for Comparison	**Moran et al., 2017**	**Demir et al., 2016**	**Tylki-Szymańska et al. 2015**	
Basic Information				
Age	17	8.8	18	8
Inheritance	*de novo*	Inherited	*de novo*	*de novo*
Dysmorphic Features				
Macrocephaly	Y	Y	Y	
Coarse Face	Y		Y	
Wide Forehead	Y	Y	Y	Y
Hypertelorism			Y	Y
Palpebral Ptosis	Y		Y	
Low or Flat Basal Bridge	Y		Y	Y
Short and Upturned Nose			Y	
Micrognathia			Y	
Macroglossia	Y			
Short Neck			Y	
Cranial Hyperostosis	Y	Y	Y	
Growth and Skeletal Abnormalities				
Delayed Growth	Y	Y	Y	
Short Stature		Y	Y	Y
Elongated Thorax			Y	Y
Lumbar Kyphosis			Y	
Short Limbs	Y	Y	Y	Y
Abnormal Foot	Y	Y	Y	Y
Abnormal Hand	Y	Y	Y	Y
Developmental Abnormalities				
IQ	**Normal**	**Mild**	**Severe (22)**	**Normal (95)**
Delayed Speech	Y	Y	Y	
Delayed Cognitive	Y	Y	Y	
Delayed Motor	Y	Y	Y	Y
Gestation Age	39+4w	N/A	41w	42w
Birth Weight	4580 g 98th centile	N/A	4200 g 90th centile	3450g >50th centile
Birth Length	56.5 cm 91st centile	N/A	56 cm >98th centile	55 cm >98th centile
Head Circumference	62.5 >99th centile	N/A	37 cm >98th centile	35 cm >75th centile

Other Features				
Deep or Hoarse Voice			Y	Y
Pale and Doughy Skin			Y	
Constipation	Y	Y	Y	Y
Anemia	Y	Y	Y	Y
Hyper-cholesterolemia	Y		Y	Y
Psychological Disorder		Y		
Biochemical Measurements				
fT4	Lower Limit	Low/Normal	Low	Low/Normal
fT3	High	High/Normal	Upper Limit	Upper Limit
TSH	Normal	Normal	Normal	Low/Normal

*3+1 and 1+1 mean that the first family has three or one cases, while the second family has one case. Table adapted from Tylki-Szymańska et al. (2015). Data adapted from Demir et al. (2016), Moran et al. (2017), and Tylki-Szymańska et al. (2015).